Carbon 216 (2024) 118503

Contents lists available at ScienceDirect

Carbon

journal homepage: www.elsevier.com/locate/carbon

Synchrotron-based UV resonance Raman spectroscopy probes size confinement, termination effects, and anharmonicity of carbon atomic wires

P. Marabotti [a,**], M. Tommasini [b], C. Castiglioni [b], S. Peggiani [a], P. Serafini [a], B. Rossi [c], A. Li Bassi [a], V. Russo [a], C.S. Casari [a,*]

[a] Micro and Nanostructured Materials Laboratory - NanoLab, Department of Energy, Politecnico di Milano, via Ponzio 34/3, I-20133, Milano, Italy
[b] Department of Chemistry, Materials and Chemical Engineering Giulio Natta, Politecnico di Milano, Piazza Leonardo da Vinci 32, I-20133, Milano, Italy
[c] Elettra Sincrotrone Trieste, S.S. 114 km 163.5, Basovizza, 34149, Trieste, Italy

A B S T R A C T

Vibrational and electronic properties and anharmonicity of sp-carbon atomic wires (i.e., polyynes) have been studied using resonance Raman spectroscopy, focusing on the confinement effects connected to their structure (length and termination). We exploited the fine tunability of the synchrotron radiation to resonantly excite short H-, CH_3-, and CN-capped carbon atomic wires at their vibronic transitions in the deep UV. We report for the first time the resonance Raman spectra of size-selected CH_3-capped polyynic wires (HC_nCH_3, n = 8–12) and CN-capped wires (HC_6CN and $HC_{12}CN$). We observed that the degree of π-electron conjugation increases with the wire length and is related to the specific termination. The analysis of multiple quanta Raman overtone bands shows that the anharmonic correction of the vibrational potential energy becomes increasingly relevant as the wire length increases. Finally, studying the vibronic lines of the UV absorption spectra allows the determination of an effective displacement parameter between the minima of the ground and the low-lying excited state, proving that the strong electron-phonon coupling of these systems is sensitive to chain length and termination.

1. Introduction

Carbon atomic wires are among the most straightforward one-dimensional systems ever synthesized, formed by linear chains of sp-hybridized carbon atoms terminated at both edges by small functional groups [1]. These systems have captivated the scientific community due to their inherent simplicity (alternated single and triple bonds in polyynes and double bonds in cumulenes), allowing us to test the theoretical predictions of the physical properties of the ideal carbyne as a limit of carbon wires of increasing length [2–7]. Their high degree of π-electron conjugation causes a strong interplay between their geometry and electronic structure, allowing for tuning their electronic, vibrational, and optical features through size confinement or proper chemical functionalization [1,8–10]. This leads to unique size-dependent opto-electronic, thermal, and mechanical properties making them highly promising for application in different technology fields [8,11–16].

Carbyne, corresponding to an infinite linear carbon wire, presents numerous fundamental unanswered questions about its properties. Its structure is expected to be polyyne-like, i.e., single-triple alternated bond configuration, due to the onset of Peierls' distortion. However, theoretical predictions indicate that the zero-point vibrational energy could overcome the potential barrier and reach the equalized bond structure configuration, making cumulene possible. Strain is expected to raise the potential barrier, leading to a stable polyyne structure [17], but strain-induced metal-to-semiconductor transition has been observed in short systems and analyzed theoretically for the ideal carbyne case [17,18]. The impact of quantum anharmonicity in determining crucial features in carbyne, such as the cumulene-to-polyyne phase transition, has been recently outlined theoretically [19]. The lack of experimental proof of carbyne's properties is due to the difficulties in synthesizing wires long enough to be considered carbyne. Carbyne is expected to display the same properties irrespective of its length, but the characteristic length setting the threshold between carbyne and carbon atomic wires affected by size confinement is still under discussion [20]. In this framework, the anharmonicity in short sp-carbon wires and how it is affected by length and termination effects is still a completely open question. The experimental availability of size- and termination-selected carbon atomic wires allows us to investigate structure-dependent

* Corresponding author.
** Corresponding author.
E-mail addresses: pietro.marabotti@polimi.it (P. Marabotti), carlo.casari@polimi.it (C.S. Casari).

https://doi.org/10.1016/j.carbon.2023.118503
Received 11 August 2023; Received in revised form 14 September 2023; Accepted 3 October 2023
Available online 4 October 2023

properties.

Raman spectroscopy emerges as a powerful tool for studying the properties of sp-carbon systems [1,21]. The analysis of the fundamental vibrational transitions of carbon atomic wires, specifically polyynes, allows for investigating their structural and nonlinear optical properties, charge transfer, optical gaps, and electron-phonon coupling [22–30]. In particular, their strong Raman-active mode, often referred to as "α mode" or Effective Conjugation Coordinate (ECC) mode, lying in a region of the Raman spectrum (*i.e.*, 1800-2200 cm^{-1}) where the other carbon allotropes are inactive, serves as a specific marker of the structure and π-electron conjugation of these systems [1,21]. It shows a significant frequency down-shift and increased Raman intensity as the wire length increases. Moreover, different chemical groups at the ends of the wire may induce detectable but weaker effects on the spectral pattern. These features depend on the wire's symmetry, which lowers in the presence of a non-symmetric capping and the dynamic coupling between the wire and its terminations [15,22,23,31]. Moreover, the involvement of atomic orbitals from the endgroups in the conjugated π-electrons system affects the electronic properties, molecular polarizability, and Raman response [3,5,31–35].

Nevertheless, the concentrations of short polyynes produced by physical synthesis methods like arc discharge and pulsed laser ablation in liquid are usually too low to be probed with conventional Raman spectroscopy [36–39]. Surface-Enhanced Raman Scattering (SERS) or resonance Raman scattering (RRS) can be exploited to overcome this issue [21,25,26,36,40–44]. In recent studies, resonance Raman scattering has shed light on the Raman excitation profile of confined carbyne, very long (up to 800 nm) linear chains confined into double-walled carbon nanotubes [45], and long linear carbon chains in multi- or single-walled carbon nanotubes [46–48], discovering size-independent optical and vibrational properties of these systems which approach the limit of the ideally infinite carbyne. Confined carbyne absorbs in the visible range and is the strongest resonance Raman scatterer ever reported [49,50]. We recently reported a deep UV resonance Raman analysis of hydrogen-capped polyynes of different lengths (from 8 to 12 carbon atoms), where we discovered a significant modulation of the Raman intensity of multiple-quanta Raman transitions by selectively exciting polyynes at specific vibronic transitions [44]. By carefully choosing the excitation wavelength, we have successfully enhanced the intensity of α mode overtones, enabling the detection of high-order transitions up to five vibrational quanta [44]. Accessing to observed frequencies of the fundamental Raman transition and its overtones opens to exploring vibrational anharmonicity as a function of structure-selected carbon atomic wires.

To significantly contribute to the ongoing discussion on anharmonicity in carbyne-like systems, in this work, we carried out an experimental and theoretical study of vibrational properties and anharmonicity of short carbon atomic wires, focusing on their modulation induced by the wire structure.

Our approach employs synchrotron-based UV resonance Raman spectroscopy and theoretical analysis by DFT methods to investigate the impact of the chain length and termination on the properties of a series of hydrogen-, methyl-, and cyano-capped carbon atomic wires in the form of polyynes. We exploited the tunability of the synchrotron radiation to exactly excite different polyynes at their corresponding absorption maxima – *i.e.,* peaks of the vibronic sequence – in the deep UV region. The resonance enhancement enables us to collect Raman spectra even from low-concentrated samples (down to $\approx 10^{-8}$ M). We reported for the first time the resonance Raman spectra of methyl- and cyano-capped wires, ranging from the fundamental transition of the α mode to its first overtone, comparing them to the simpler H-capped polyynes. This study extends previous work on resonance Raman spectroscopy of H-capped polyynes [44] to explore the effect of terminations.

By analyzing the UV absorption spectra, we estimated the dimensionless effective displacement parameters of the different species and discussed the impact of specific terminations on the electron-phonon coupling in these systems. Moreover, the analysis of second-order Raman spectra, including higher orders for the HC_nH series, allowed us to discuss the anharmonicity of the main Raman mode (i.e., α mode) and its dependence on wires' size and terminations. We observed a steep increase in the anharmonic character of the vibrational potential in longer chains, which is further supported by DFT calculations of the potential energy surface (PES) along the ECC coordinate of HC_nH wires of increasing length.

Our results highlight significant anharmonicity in carbon atomic wires with an increasing trend with the wire length. Such large anharmonicity can affect thermal expansion and strain effects, potentially exploitable in future nanoelectronics and thermoelectricity. The linear increase observed up to 26 carbon atoms indicates that the onset for the carbyne limit is still far, and an even larger anharmonicity could be expected for ideal carbyne. However, carbon atomic wires represent an intriguing class of systems with unique property modulation opening to applications as a quantum material.

2. Methods

Polyynes' solutions were prepared following the experimental procedure described in previous work [36]. A mixture of polydisperse polyynes, characterized by various wire lengths and terminations, was synthesized in acetonitrile through pulsed laser ablation in liquid [36]. They were separated in monodispersed solutions of acetonitrile and water by high-performance liquid chromatography (HPLC). We collected their size- and termination-selected UV-Vis absorption spectra during the separation. Cyano-capped polyynes (HC_nCN, with n = 6, 8, and 10) were transferred in cyclohexane after HPLC with a liquid-liquid extraction method to avoid the overlap of the α mode of n = 6 chain and their CN stretching modes with the CN stretching mode of acetonitrile.

UV resonance Raman (UVRR) spectra were collected by exploiting the synchrotron-based UVRR set-up available at the BL10.2-IUVS beamline of Elettra Sincrotrone Trieste (Italy) [51]. All the samples were measured employing the experimental method described in Ref. [44]. Different excitation wavelengths in the deep UV range were exploited (see Table S1 in the SI), provided by the emission of synchrotron radiation (SR), by accurately changing the aperture of the undulator gap. The SR light has been then monochromatized by using a 750 cm focal length spectrograph equipped with a holographic grating of 3600 groves/mm. Raman spectra corresponding to excitation at the vibronic peaks above 272 nm (and below 200 nm) were not measured due to limitations of the minimum undulator gap aperture. The radiation power on the samples ranges from a few up to tens of μW (see Table S1). The calibration of the spectrometer was performed using the CH_2 scissoring mode of cyclohexane (spectroscopic grade, Sigma Aldrich) at 1444.4 cm^{-1}. The final spectral resolution depends on several contributions: the resolving power of the SR monochromator (focal length, grating, slits aperture) and the analyzer (750 cm focal length, 1800 g/mm), the excitation wavelength, and the spectral range – determined by the pixel spacing of the CCD. For each excitation wavelength, a reliable estimation of the final resolution of the collected Raman spectra can be given by a general equation $(spectral\ range\ [cm^{-1}])/1340$ (for instance, 2.6, 1.9, and 1.6 cm^{-1}/pixel at 216, 251, and 272 nm of excitation wavelengths, respectively).

We excited polyynes at their corresponding strongest vibronic line associated with the fundamental $|0\rangle_g \rightarrow |0\rangle_e$ transition, namely between the low-lying ($|m = 0\rangle$) vibrational level of the ground (g) electronic state and the lowest-energy vibrational level ($|k = 0\rangle$) of the first dipole-allowed excited (e) electronic state. The only exceptions, due to the wavelength-limitations of the synchrotron-based deep UV tunable source, are $HC_{12}CH_3$ wire, which was excited at the $|0\rangle_g \rightarrow |1\rangle_e$ transition, $HC_{10}CH_3$ wire, which Raman spectra were collected in resonance with the $|0\rangle_g \rightarrow |0\rangle_e$ and $|0\rangle_g \rightarrow |1\rangle_e$ transitions, and $HC_{12}CN$ and $HC_{14}H$ wires, excited in resonance with the $|0\rangle_g \rightarrow |2\rangle_e$ vibronic peak. Table S1 reports

additional information concerning the UV absorption and resonant Raman measurements carried out on the set of molecules.

Density functional theory (DFT) simulations were performed on single linear chains using Gaussian09 [52]. PBE0/cc-pVTZ calculations were used for the computation of the Raman spectra. Indeed, PBE0/cc-pVTZ has been shown to provide a good agreement with experiments when used to compute the Raman spectra [1,21,22,36,53]. DFT Raman spectra have been uniformly scaled by a factor of 0.9512. This value is an average of the scaling factor needed to match the experimental and calculated α modes of H–capped polyynes [44]. With the same computational setup, we investigated for HC_nH wires (n = 8–26) the anharmonic contribution to the PES while varying the ECC coordinate.

3. Results

3.1. UV–Vis absorption and UV resonance Raman spectra

Fig. 1 reports the UV–Vis absorption spectra of hydrogenated carbon wires from our previous work [44] and CH_3– and CN–capped polyynes extracted during the separation process from the diode array detector of the HPLC, *i.e.*, in acetonitrile-water solutions. To identify the corresponding species in each spectrum, we compared them with the literature [36,54,55] and TD-DFT calculations [36]. The sequence of sharp peaks in the UV region of H–capped polyynes corresponds to the vibronic progression associated with the dipole-allowed $^1\Sigma_u^+ \leftarrow X^1\Sigma_g^+$ transition. This transition involves excitations between the first vibrational level of the ground state ($|0\rangle_g$) and the different vibrational levels of the first excited states ($|k\rangle_e$). The most intense peak corresponds to the $|0\rangle_g \rightarrow |0\rangle_e$ excitation, while the others match transitions to vibrational levels at higher vibrational quantum numbers (k). The absorption spectra of CH_3– and CN–capped polyynes display distinct features on the longer wavelength side of the $|0\rangle_g \rightarrow |0\rangle_e$ line. Specifically, CH_3–capped wires show a shoulder merged with the $|0\rangle_g \rightarrow |0\rangle_e$ peak, while CN–capped polyynes display a weak vibronic pattern. These features arise from the symmetry breaking caused by hetero-terminations in CH_3– and CN–capped polyynes, allowing electronic transitions that are symmetry-forbidden in linear, centrosymmetric ($D_{\infty h}$ symmetry group) H–capped species [27,56]. Despite this, the overall shape of the absorption spectra of CH_3–capped polyynes resembles that of H–capped chains with the same n, indicating a relatively weak perturbation from the methyl group. Instead, absorption spectra of HC_nCN wires are significantly red-shifted compared to hydrogen-capped species with the same n. This experimental evidence suggests the involvement of the CN group in the delocalized π-electrons system, resulting in an intermediate effective conjugation length of HC_nCN between HC_nH and $HC_{n+2}H$. Moreover, especially for HC_6CN and HC_8CN, the vibronic sequence may be affected by the vibrational structure of different electronic states and potentially involve the contribution of vibronic transitions different from the Raman-active α mode.

To obtain the UVRR spectrum of specific wires, we selected the excitation wavelength according to the absorption spectrum's vibronic progression (see Fig. 1 and Table S1). The limitations imposed by the characteristics of the undulator and the beam transport system of the IUVS beamline narrow the tunability of the Raman excitation between 200 and 272 nm. Within this range, we successfully probed H–capped polyynes (HC_nH) with n = 8–14, CH_3–capped polyynes (HC_nCH_3) with n = 8–12, and CN–capped polyynes (HC_nCN) with n = 6–12. The UVRR spectra of the ten selected polyynes are shown in Fig. 2. The excitation wavelengths we adopted for investigating each system are listed in Table S1 in the SI. In some cases, we used different excitation wavelengths to probe fundamental and multiple quanta vibrational transitions, *i.e.*, we picked up resonances at different $|0\rangle_g \rightarrow |k\rangle_e$ ($k > 0$) transitions. This ensures obtaining more effective resonance enhancement in specific spectral regions (*i.e.*, the first- or higher-order Raman range), as discussed in our previous work [44]. Each panel of Fig. 2 reports the spectra of polyynes with different lengths but the same termination. The intensities of each species are normalized to the α or 2α lines. In the first-order Raman spectra of H– and CH_3–capped wires, the CN stretching mode of acetonitrile (solvent) prevents the analysis above 2230 cm^{-1}. Moreover, in the second-order Raman spectra of long H– and CH_3–capped carbon wires, we notice the presence of two vibrational lines, centered at about 4035 and 4320 cm^{-1}, assigned to overtones of characteristic Raman transitions of acetonitrile (black asterisks in the second-order Raman region of Fig. 2) [44]. These modes are visible only in the least concentrated samples where the intensity of their 2α lines is comparable to that of acetonitrile's overtones. Three- and four-quanta

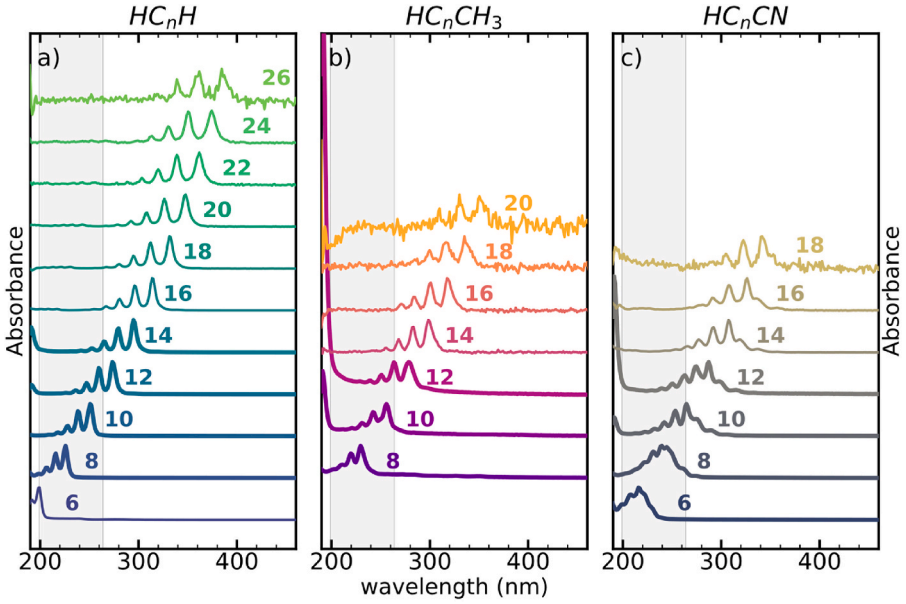

Fig. 1. UV–Vis absorption spectra of a) H–capped polyynes (HC_nH, n = 6–26), b) CH_3–capped polyynes (HC_nCH_3, n = 8–20), and c) CN–capped polyynes (HC_nCN, n = 6–18). The grayed region from 200 nm to 272 nm highlights the region accessible through the UVRR setup available on IUVS due to instrumental limitations of the undulator. The bolder spectra highlight polyynes measured with UVRR (see Fig. 2). (A colour version of this figure can be viewed online.)

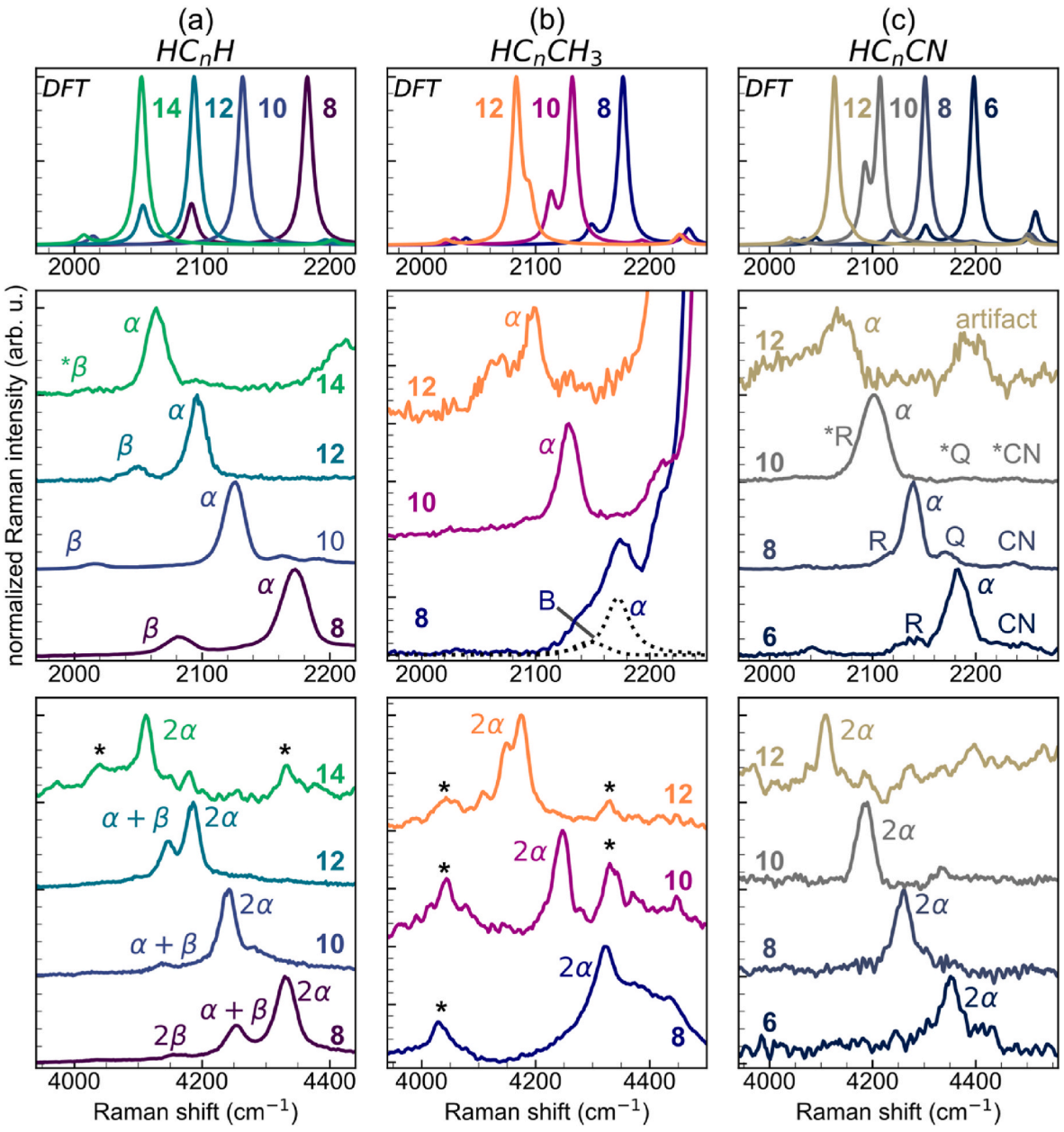

Fig. 2. Multi-wavelengths experimental UVRR spectra of H–capped (panel a, HC_nH, n = 8–14), CH_3–capped (panel b, HC_nCH_3, n = 8–12), and CN–capped (panel c, HC_nCN, n = 6–12) polyynes. DFT simulations of Raman spectra of the same chains are reported in the top panels (frequency scaling factor of 0.9512). Experimental first- and second-order Raman spectra are shown in the middle and bottom series of panels, respectively. The excitation wavelengths employed for recording first- and second-order Raman spectra are reported in Table S1 in the SI. In the first-order region of HC_8CH_3, the result of curve fitting is shown to help visualize the Raman bands, which are partially hidden due to the overlap with the intense CN peak of acetonitrile. The visible normal modes analyzed in the main text are labeled (α, β, B, R, Q, and CN), prepending an asterisk if they have low intensity or merge with other peaks. Overtones of acetonitrile in the second-order region are highlighted with black asterisks. (A colour version of this figure can be viewed online.)

Raman transitions of H–capped polyynes are shown in the SI in Fig. S1a and b, respectively. The top panels of Fig. 2 compare experimental first-order Raman spectra to DFT simulations (see Methods for scaling details).

The α mode of polyynes exhibits the highest intensity in the first-order region of Fig. 2 (2000–2200 cm^{-1}) [21,25,44]. This mode involves a collective motion of all the CC bonds in the *sp* skeleton, characterized by the simultaneous shrinking of the single and stretching of the triple bonds [21,25]. Fig. 3 shows the relationship between the experimental wavenumbers of the α mode (ν_α) and the effective conjugation length (n^*), where $n^* = n$ for HC_nH and HC_nCH_3 and $n^* = n+1$ for HC_nCN (the corresponding ν_α values are listed in Table S2). For the whole set of molecules, n^* corresponds to the number of consecutive sp-hybridized carbon atoms. Within each series of H–, CH_3–, and CN–capped polyynes, the α mode frequency down-shifts as the chain length increases, reflecting the expected increase of π-electron conjugation. H-capped polyynes possess an additional weaker satellite peak at frequencies below the α mode (see Fig. 2a), assigned to the so-called β mode [21,25,43,44]. This vibration has a more complex pattern than the α mode's one and can be described as an out-of-phase collective motion of the CC triple bonds in the chain [21,25], with a variable contribution from the stretching of the single CC bonds, depending on the chain length. The experimental frequency of the β mode (ν_β, see Table S2) shows oscillatory behavior with increasing chain length (see Fig. 3),

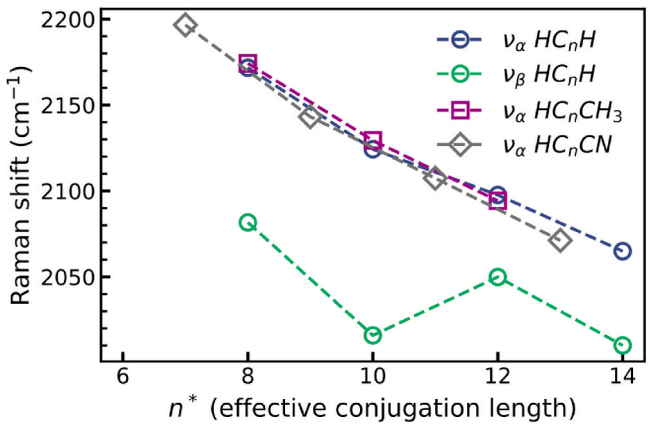

Fig. 3. Experimental frequency dispersion of the α mode (ν_α) of polyynes as a function of the effective conjugation length (n^*). $n^* = n$ for HC_nH and HC_nCH_3, while $n^* = n + 1$ for HC_nCN polyynes. The frequency dispersion of the β mode (ν_β) of H–capped polyynes is reported as well.

consistent with previous findings by Tabata et al. [25] and confirmed by DFT calculations (Fig. 2a). In particular, ν_β shows a monotonic decreasing trend with n when considering wires with odd and even numbers N of C ≡ C bonds separately ($N = n/2$). The intensity of the β mode diminishes from HC_8H to $HC_{14}H$, becoming barely visible in $HC_{14}H$ (Fig. 2a). Indeed, this Raman-active vibration is a result of size confinement, and it vanishes by approaching the ideal carbyne limit, which features a single Raman-active ECC mode (*i.e.*, the α mode phonon at $\boldsymbol{q} = \mathbf{0}$ wavevector) [1,20,21,44,57].

To the best of our knowledge, we report, for the first time, the resonance Raman spectra of size-selected methyl-capped polyynes ranging from HC_8CH_3 to $HC_{12}CH_3$. These spectra are dominated by the α band, which matches the prediction of DFT calculations for methyl-capped polyynes (see Fig. 2b and Table S2). This confirmation validates the assignment of these spectra to methyl-capped polyynes, which was previously determined by UV–Vis spectroscopy [36,55]. From Fig. 3, we observe that the experimental frequencies of the α band of CH_3–capped polyynes are very close to those of H–capped chains of the same length (same n^*). This observation suggests that the methyl group minimally impacts the degree of π-electron conjugation. This is quite surprising because of the well-known electron-donating properties of the CH_3 group. Indeed, it usually gives rise to hyperconjugation phenomena when linked to groups containing π-electrons, such as C=C, C ≡ C, and aromatic rings [3,21,28,35,58,59]. DFT predictions indicate a remarkable reduction in the bond length of the CC unit connected to the methyl group in methyl-capped wires (d_{C-CH_3} ranging from 1.449 Å for HC_8CH_3 to 1.448 Å for $HC_{18}CH_3$) compared to the typical bond length of a CC single bond (e.g., for ethane $d_{C-C} = 1.528$ Å) [60]. Moreover, the wavelengths of the $|0\rangle_g \rightarrow |k\rangle_e$ transitions, observed in the UV absorption spectra of HC_nCH_3 wires, show a consistent red-shift (of about 4 nm) compared to HC_nH (see Table S1). The analysis of the computed vibrational eigenvectors (Figure S2) suggests that the stretching of the C-C bond (R_{C-CH_3}) linking the CH_3 group to the polyyne chain barely participates in the collective ECC mode responsible for the α band. Indeed, despite HC_nCH_3 wires contain $n + 1$ carbon atoms, which are to some extent incorporated in the π-electron system, the weak dynamical coupling between the ECC vibration and R_{C-CH_3} effectively confines the α mode within the polyyne segment formed by n carbon atoms, preventing any detectable influence of the hyperconjugation from the methyl group on the position of the α mode.

DFT calculations of the Raman spectra of CH_3–capped chains confirm the dynamic coupling between the R_{C-CH_3} stretching vibration and other-than-ECC-like vibrations of the polyyne chain, which gives rise to satellite Raman peaks. The two main satellite bands, occurring at a lower frequency and higher frequency than the α band for HC_8CH_3 and $HC_{10}CH_3$, are highlighted in Fig. 4a as B and C modes, respectively. Their vibrational eigenvectors, illustrated in Fig. S2, show that the B and C modes involve the stretching of triple and single bonds along the *sp*-chain, coupled with the CC stretching of the methyl group. The C mode, in particular, shows larger bond stretching on the portion of the sp-chain closer to the CH_3 group, showing a small or even vanishing contribution from the CC bonds' stretching near the H capping. Fig. 4b shows their theoretical dispersion (ν_B and ν_C) as a function of n^*. The B mode displays a significant monotonic frequency decrease with increasing chain length, while the C mode only slightly down-shifts from 2234 to 2227 cm^{-1}. The vibrational eigenvectors in Fig. S2 reveal that the C mode represents the Raman-activated IR-active ECC-like mode with a node at the center of the chain. Previous studies have observed the activation of the IR ECC modes in Raman spectra of non-centrosymmetric polyynes due to polarization effects along the π-conjugated chain [23]. The B mode, displaying a partial ECC character, accounts for its remarkable frequency dispersion with n^*. However, the decreasing trend of the B frequency is less steep than that of the α line, and for $HC_{12}CH_3$, an inversion of the relative position of the two bands occurs between n = 10 and n = 12.

Experimentally, detecting satellite peaks is challenging due to the low concentration of polyynes in the samples. Only the B mode of HC_8CH_3 can be faintly observed at ≈2147 cm^{-1} (scaled DFT wavenumber: 2149 cm^{-1}), appearing as a shoulder of the α band (see Fig. 2b). The intense CN stretching peak of acetonitrile (solvent) overshadows C modes. Unfortunately, the choice of the solvent is limited by the HPLC collection method, and subsequent liquid-liquid extraction methods further decrease polyynes' concentration, consequently reducing their Raman intensities.

Considering now cyano-capped polyynes, we show the UVRR spectra of HC_6CN to $HC_{12}CN$ in Fig. 2c. To the best of our knowledge, this study marks the first observation of the Raman spectra of HC_6CN and $HC_{12}CN$, whereas our UVRR spectra for n = 8 and 10 align well with previous findings [27]. In terms of the α modes of cyano-capped polyynes (Fig. 3), we observed an average frequency down-shift of approximately 30 cm^{-1} compared to the α modes of H–capped polyynes with the same number of CC triple bonds (see also Table S2). Indeed, the cyano termination is involved in π electrons orbitals and enhances the π-electron conjugation path, as observed in other polyynes carrying endgroups with π electrons [61–65]. This effect is particularly notable in cyano-capped polyynes, where the position of the α line reflects the extension of the characteristic ECC atomic displacement pattern throughout the entire conjugation path, including the stretching of the terminal C–CN bond (see Fig. S2). As observed previously in our analysis of the UV–Vis spectra, by associating an effective conjugation length $n^* = n + 1$ to each cyano-capped polyyne (Fig. 3), we can establish a common dispersion trend for the frequencies of the α mode of hydrogen- and cyano-capped polyynes. This implies that the CN group contributes to the conjugation length equivalently to one-half of an additional triple bond. Two possible explanations arise for this behavior: firstly, the nitrogen atom's higher electronegativity allows for more effective pinning of its p_z electron, making it less effective than an sp-carbon atom in increasing π-electron conjugation (i.e., extending the conjugation length by $n + 1$ instead of $n + 2$ as with a CC triple bond); secondly, the contribution of the CN stretching to the collective α mode is smaller or negligible compared to an additional C ≡ C bond, limiting its effect on the position of the α line.

Like the case of the methyl group, the CN termination generates satellite peaks in the frequency range of the α mode, as observed in DFT simulations reported in Fig. 4c. The calculations predict the presence of low-frequency (R) and high-frequency (Q) satellite peaks and their frequency dispersion with the chain length is shown in Fig. 4d. The vibrational eigenvectors sketched in Fig. S2 in the SI show that the R mode presents a CC stretching pattern of the sp-chain similar to that of the B mode of the CH_3–capped molecules. Again, the stretching of the endgroup (*i.e.*, of the CN bond) shows a remarkable contribution to the

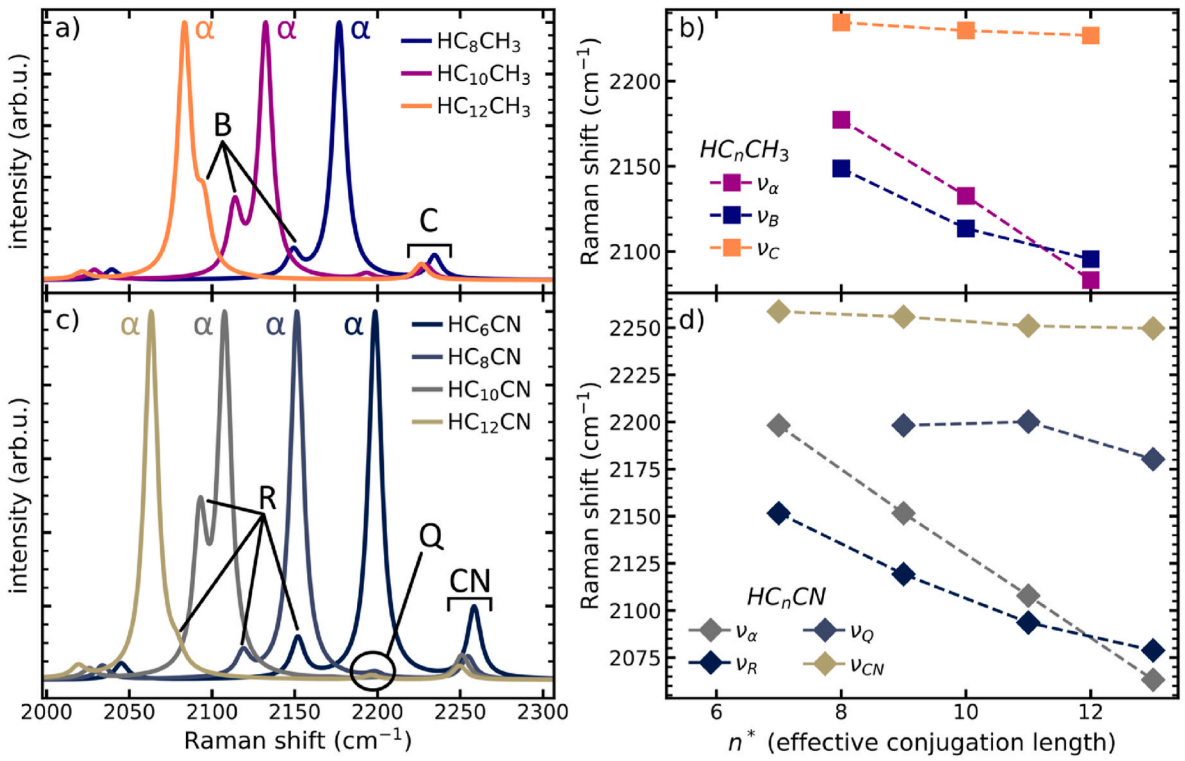

Fig. 4. a) Raman spectra of methyl-capped polyynes (HC_nCH_3) from DFT calculations. The normal modes analyzed in the main text are labeled (α, B, and C) and their predicted frequency dispersions with the effective chain length are reported in panel b) as ν_α, ν_B, and ν_C, respectively. c) Raman spectra of cyano-capped polyynes (HC_nCN) from DFT calculations. The normal modes analyzed in the main text are labeled (α, R, Q, and CN) and their frequency dispersions with the effective chain length are reported in panel d) as ν_α, ν_R, ν_Q, and ν_{CN}, respectively.

vibrational eigenvector. This is different from the case of the Q vibration, a collective CC stretching with one central node, characterized by a small contribution of the CN stretching, which vanishes for the longest chain.

The dispersion of the lower frequency R mode is more pronounced than that of the higher frequency Q mode, although less steep compared to the α band. In $HC_{10}CN$, the R and α frequencies are very close, while in $HC_{12}CN$, their relative positions are inverted (see Figs. 2c and 4d). Interestingly, the CN stretching, which participates in the π electrons system, undergoes a slight frequency modulation from 2259 (HC_6CN) to 2250 cm^{-1} ($HC_{12}CN$), as illustrated in Fig. 4c and d. Indeed, DFT calculations reveal that this mode is essentially localized on the C−CN group (Fig. S2). Experimentally, the satellite Raman peaks (R, Q, and CN modes) are detected in the Raman spectra of HC_6CN and HC_8CN only, in agreement with DFT calculations. Instead, the R mode of $HC_{10}CN$ is not resolved and appears as a small band preceding the α mode (see Fig. 2c).

3.2. Electronic excitation: vibronic structure and electron-phonon coupling

To further investigate the size confinement effect, we have evaluated the effective nondimensional displacement parameter (δ_{eff}, Fig. 5) from the experimental UV–Vis spectra of size-selected polyyne (Fig. 1) [44,66], which is proportional to the distance between the minima of the potential energy surfaces of the ground and low-lying electronic excited state. This parameter determines the resonance Raman activity and the pattern of the UV–Vis absorption spectrum of the molecules, and it is related to their electron-phonon coupling [2,25,44,67–69]. The displacement parameter is connected to the Huang-Rhys factor (S) via the following relation [66–68], which is valid in a simplified "one--mode" approximation:

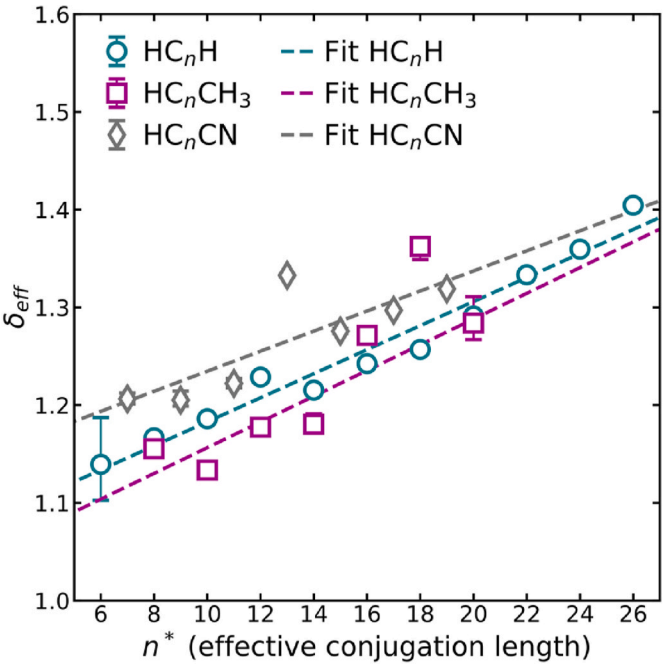

Fig. 5. Nondimensional effective displacement parameter for hydrogen- (greenish circles), methyl- (pinkish squares), and cyano-capped (grayish diamonds) polyynes extracted from the UV–Vis spectra of Fig. 1. The error bars are due to the error of the fit model used to deconvolve the UV–Vis absorption spectra. Linear trends are reported by dashed lines for the three series of polyynes. The linear trend for methyl-capped polyynes was found by excluding the off-scale value of $HC_{18}CH_3$. (A colour version of this figure can be viewed online.)

$$\delta_{eff} = \sqrt{2S} = \sqrt{2\frac{I_{0\to1}}{I_{0\to0}}} \quad \text{(Eq. 1)}$$

According to Eq. (1), the Huang-Rhys factor can be extracted from the UV–Vis absorption spectrum and is defined as the ratio of the absorbance of the $|0\rangle_g \to |1\rangle_e$ ($I_{0\to1}$) and $|0\rangle_g \to |0\rangle_e$ ($I_{0\to0}$) transitions [44, 66]. In solid state systems, the Huang-Rhys factor quantifies the average number of vibrational quanta generated in an electronic transition, quantifying the electron-phonon coupling of crystals [70].

In this framework, we assume a one-mode approximation to describe the vibronic structure of the UV–Vis absorption spectrum by considering the α mode only. For this reason, we call "effective" the displacement parameter we obtained [44]. While other collective modes may exist, their contributions are significantly weaker than the α mode, which exhibits the highest Raman activity and electron-phonon coupling and is responsible for the intensity pattern and peak position of the vibronic sequence of polyynes. The effective displacement parameters of H–capped wires shown in Fig. 5 are obtained from Ref. [44]. Conversely, the displacement parameters for CH_3– and CN–capped polyynes were calculated from Eq. (1). This involved extracting the absorbance of the vibronic transitions ($I_{0\to1}$ and $I_{0\to0}$) by fitting the UV–Vis absorption spectra (Fig. 1) with a multi-Lorentzian function with a linear baseline correction. Despite potential errors arising from fitting noisy absorption spectra (see Fig. 1), we observed a consistent trend across all three series of systems: the displacement parameters increase with the wire length, regardless of the termination. This observation further supports the correlation between electron-phonon coupling and π-electron conjugation, as observed in H–capped polyynes [44].

We analyzed the trend of δ_{eff} vs. n^* in each series of polyynes by fitting them with a linear relationship. The results indicate that cyano- and methyl-capped polyynes have slightly larger and slightly smaller δ_{eff} values, respectively, than hydrogen-capped polyynes of similar length. Within the limitations of the one-mode approximation, the systematic higher values for HC_nCN suggest a little larger electron-phonon coupling compared to other polyynes chains. This effect diminishes with increasing the chain length, and the corresponding displacement parameters approach that of hydrogen-capped polyynes. Our values tend towards but remain lower from the limit of carbyne, observed experimentally for nanotube-confined carbyne, which is approximately 1.92 (derived from a Huang-Rhys factor of 1.82) [45].

3.3. Size- and termination-dependent anharmonicity

Beyond the characteristic CH modes of the solvents, *i.e.*, $\nu > 3600$ cm^{-1}, we detected vibrational lines at approximately twice the frequency of the α mode [44,71]. We assigned these signals to the first overtone of the α mode and combination bands involving the α mode and other collective modes mentioned before [44]. In the case of H-capped polyynes, we observed high-order overtones (3α and 4α modes), reported in Fig. S1 in the SI. Considering methyl-capped chains, the lack of high-order overtones is caused by the low sample concentration compared to the others (see Table S1 in the SI). Instead, the cyano termination makes CN–capped polyynes more unstable [36,54]. Thus, their concentration (Table S1 in the SI), obtained just after their synthesis, can be overestimated, and their stability under UV irradiation may be more reduced than other chains. For these reasons, we cannot detect the 3α and 4α modes in these systems.

As discussed in the following, the positions of the α mode overtones shift to lower frequencies as the π-electron conjugation increases, as shown in Fig. 6, Fig. S1c and d for 2α, 3α, and 4α modes, respectively (see Table S2 in the SI). More importantly, for all the systems, the frequency of the 2α line is lower than two times that observed for the fundamental transition, highlighting the anharmonicity of the $v = 2$ vibrational levels. The 2α lines of methyl- and hydrogen-capped polyynes show similar frequencies up to a length of 10 carbon atoms (see Fig. 6). Considering cyano-capped polyynes, we still observe a decreasing trend when plotting the frequencies of the 2α lines vs. n^*. This trend is similar to that of the HC_nH series (Fig. 6), but the frequency values for cyano-capped wires deviate from those of the H–capped series, showing a non-negligible shift in the trend line of $\Delta\nu \cong -20$ cm^{-1}. Specifically, the $\nu_{2\alpha}$ values of HC_nCN with $n^* = 7, 9, 11$ are close to the $\nu_{2\alpha}$ values of H-capped wires with one additional carbon atom, corresponding to $n^* = 8, 10, 12$ (see Fig. 6 and Table S2). However, the 2α line of $HC_{12}CN$ ($n^* = 13$) does not follow this pattern, showing a $\nu_{2\alpha}$ value that is further down-shifted by 8 cm^{-1} compared to $HC_{14}H$ ($n^* = 13 + 1$, see Fig. 6). These observations suggest that the degree of anharmonicity of the α mode depends not only on the effective conjugation length (n^*), but it is also significantly influenced by the termination.

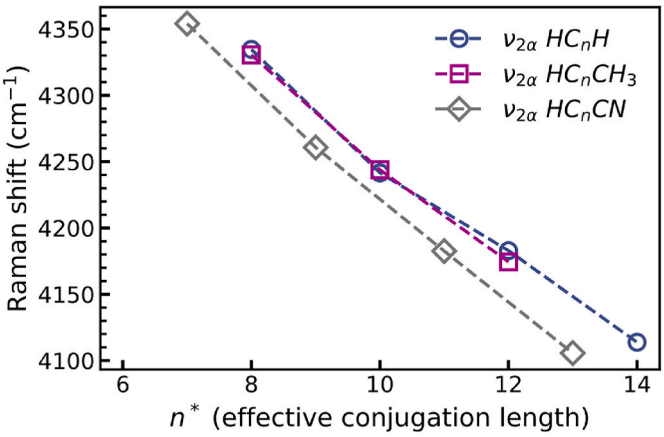

Fig. 6. Experimental frequency dispersion of the 2α mode ($\nu_{2\alpha}$) of polyynes as a function of the effective conjugation length (n^*). $n^* = n$ for HC_nH and HC_nCH_3, while $n^* = n + 1$ for HC_nCN polyynes.

We exploited the detection of Raman overtones to estimate the anharmonicity of the α mode of polyynes. From the experimental energy spacing of the vibrational energy levels in the ground electronic state of the α mode (see Table S3 in the SI), which is derived from the frequencies of its fundamental Raman transition and overtones in UVRR spectra (see Table S2 in the SI), we can estimate an anharmonic nondimensional parameter (χ) and the α mode frequency ($\nu_{\alpha,harm}$) that is associated with the harmonic approximation of the potential energy surface of these wires [72]. In the single mode approximation, χ appears in the expression of the vibrational energy levels, according to this relationship [73]:

$$\frac{E_m}{hc} = \varepsilon_0 + \widetilde{\nu}_{harm} m - \widetilde{\nu}_{harm}\,\chi\,(m^2 + m) \quad \text{(Eq. 2)}$$

The calculations' details are described in the SI, where the values of χ and $\nu_{\alpha,harm}$ are reported in Table S4 in the SI. As discussed in the SI, we used the frequencies of the fundamental transition and the first overtone (2α) of the α mode to establish a system of two equations starting from Eq. (2), enabling us to determine χ and $\widetilde{\nu}_{harm}$ (see Eq. S.5 in the SI). The resulting χ values are reported in Fig. 7a, while Fig. 7b shows the distance (in cm^{-1}) between the experimentally observed frequency of the fundamental α mode and its harmonic counterpart ($\nu_\alpha - \nu_{\alpha,harm}$). For H–capped polyynes only, an alternative approach allows us to extract χ and $\nu_{\alpha,harm}$, involving a linear regression procedure (Eq. S.7 in the SI), exploiting the availability of the experimental frequencies of higher-order overtones (3α and 4α). The results of such a procedure are illustrated in SI (Fig. S3).

The anharmonic parameters χ (Fig. 7a) and $\nu_\alpha - \nu_{\alpha,harm}$ (Fig. 7b) exhibit an increasing trend with the wire length, confirming that higher conjugation of the π electrons effectively enhances the anharmonicity of the α mode. However, a slight deviation from this trend is observed for systems with $n = n^* = 10$ (HC_nH and HC_nCH_3) and $n^* = 11$ (HC_nCN), which may be related to some weakness of the experimental

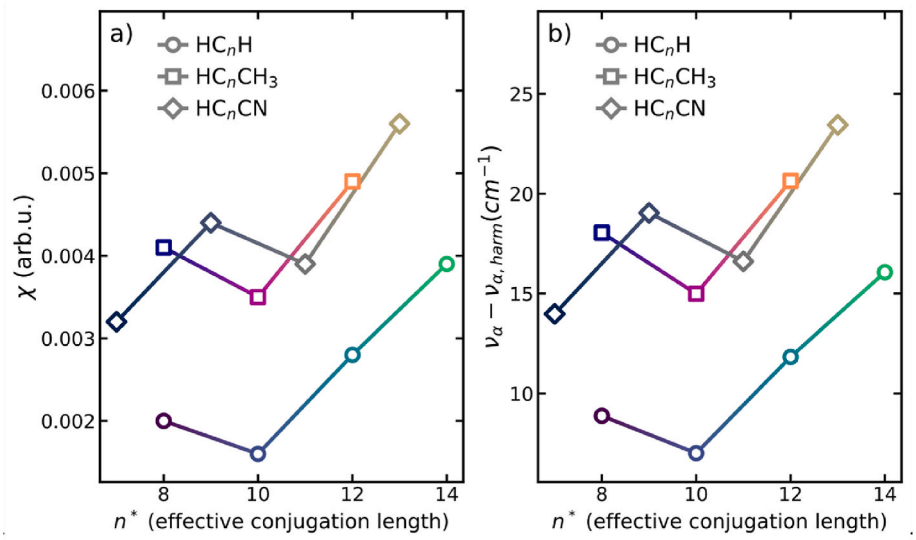

Fig. 7. a) Anharmonic nondimensional parameter (χ) for hydrogen- (circles), methyl- (squares), and cyano-capped (diamonds) polyynes. χ are calculated using Eq. S.5 and the data reported in Table S2 in the SI. b) Difference between the fundamental α mode frequency observed experimentally (ν_α, see Table S2) and its harmonic complement ($\nu_{\alpha,harm}$) for hydrogen- (circles), methyl- (squares), and cyano-capped (diamonds) polyynes. $\nu_{\alpha,harm}$ are calculated using Eq. S.5 and the data in Table S2 in the SI.

determination of the frequencies of α and 2α modes. To mitigate this, we carefully selected the excitation wavelength to optimize the signal-to-noise ratio in the spectrum's first- or second-order regions. Unfortunately, comparing spectra collected in resonance with different vibronic transitions (e.g., different k of the $|0\rangle_g \rightarrow |k\rangle_e$ transition) introduces a potential source of error, as a small shift (1 cm^{-1}) in the position of either the α or 2α lines induces significant (≈10 %) variations in evaluating χ. Nevertheless, when using α and 2α modes collected with the same excitation wavelength (i.e., same UVRR spectrum), the χ values display non-negligible dispersions, as shown by the error bars in Fig. S4 in the SI. Additionally, the accuracy in resolving the correct position of the 2α lines within the multicomponent second-order feature (comprising the α + β and 2β transitions) introduces another potential source of error.

Fig. 7a demonstrates that the anharmonic parameters of hetero-capped wires are approximately double those of hydrogenated polyynes with the same effective length. Similarly, as reported in Fig. 7b, the displacement between the harmonic (extracted from the model) and *anharmonic* (experimental) frequencies widens with increasing wire length. While our analysis reveals a correlation between polyynes' anharmonicity and their degree of π-electron conjugation, the impact of terminations seems more intricate. However, even considering experimental uncertainties in determining the position of the 2α line and the limitations of the one-mode approach, we observe increased anharmonicity in the first overtone due to symmetry breaking induced by different capping groups. Hence, our results indicate a significant role of the endgroups in determining the anharmonicity of the ECC vibration.

To delve further into the significant connection between the anharmonicity of the ECC vibration and conjugation length, we conduct a comprehensive theoretical investigation using DFT to explore the potential energy surface of HC$_n$H polyynes spanning from $n^* = 8$ to $n^* = 26$. This analysis will offer us a theoretical estimation of χ, allowing us to compare and enhance our understanding of polyynes' anharmonicity in light of the experimental findings discussed thus far.

To investigate the anharmonic features of the α (ECC) mode in HC$_n$H polyynes, we calculated the intramolecular potential energy (V) as a function of the normal coordinate of the α mode (q_α), that is the projection of the Potential Energy Surface (PES) along the ECC mode. We determined the vibrational frequencies and normal modes for the HC$_n$H polyynes ($n^* = 8 - 26$). To assess the anharmonicity, we displaced the optimized geometry of each polyyne wire from the minimum along the ECC normal coordinate in the interval [-0.4, 0.4] Å amu^{½} with a spacing of 0.01 Å amu^{½}. For each displaced geometry, we computed the energy (E) following the procedure illustrated in the SI. The inset of Fig. 8a shows the energy *vs.* q_α curves. To facilitate the comparison of all polyynes, we adopted non-dimensional quantities: a dimensionless normal coordinate $t = \left(\frac{\omega_\alpha}{\hbar}\right)^{\frac{1}{2}} q_\alpha$ represents the vibrational coordinate, and the potential energy $\overline{V} = [E(q_\alpha) - E(0)]/(\hbar\omega_\alpha)$ is measured in units of vibrational quanta.

By plotting the actual values of $\overline{V}$ from the PES calculation for HC$_n$H against the t coordinate, we obtain a stack of curves that deviate from the typical harmonic parabola described by the universal relationship:

$$\overline{V}^{harm}(t) = \frac{1}{2}t^2 \qquad \text{(Eq. 3)}$$

The PESs of the HC$_n$H series exhibit increasing anharmonicity as the wire length (n^*) increases, deviating progressively from the harmonic PES. This intriguing behavior aligns with the unusual anharmonicity recently discovered in carbyne [19], based on first-principle calculations within periodic boundary conditions. Considering the phase of t as defined in the caption of Fig. 8, we observe higher anharmonicity in longer polyynes for positive t values that describe geometry changes towards cumulenic structures. This observation tells us that the increasing anharmonicity of the ECC coordinate with n^* provides empirical evidence of the effectiveness of the chain length in modulating the energy landscape of the transition from a polyynic to a cumulene-like structure. By estimating the anharmonic parameter, we could gain valuable insight into the specific influence of the chain length on this phenomenon.

Fig. 8a shows the increase ($\Delta E(\tilde{t}) = E^{harm}(\tilde{t}) - E^{anharm}(\tilde{t})$) in the (anharmonic) contribution to the PES at $\tilde{t} = \sqrt{5} \approx 2.24$, corresponding to the classical turning point of the vibrational level $v = 2$ of the harmonic oscillator ($E^{harm}_{v=2} = 2.5$). This increase grows passing from shorter systems (HC$_8$H with $\Delta E(\tilde{t}) = 0.20$) to longer wires (HC$_{26}$H with $\Delta E(\tilde{t}) = 0.33$), paralleling the experimental behavior of the two-quanta Raman transitions, which also display increased anharmonicity in longer polyynes.

Further evidence of the connection between anharmonicity and n^* is obtained by estimating the non-dimensional anharmonicity parameters

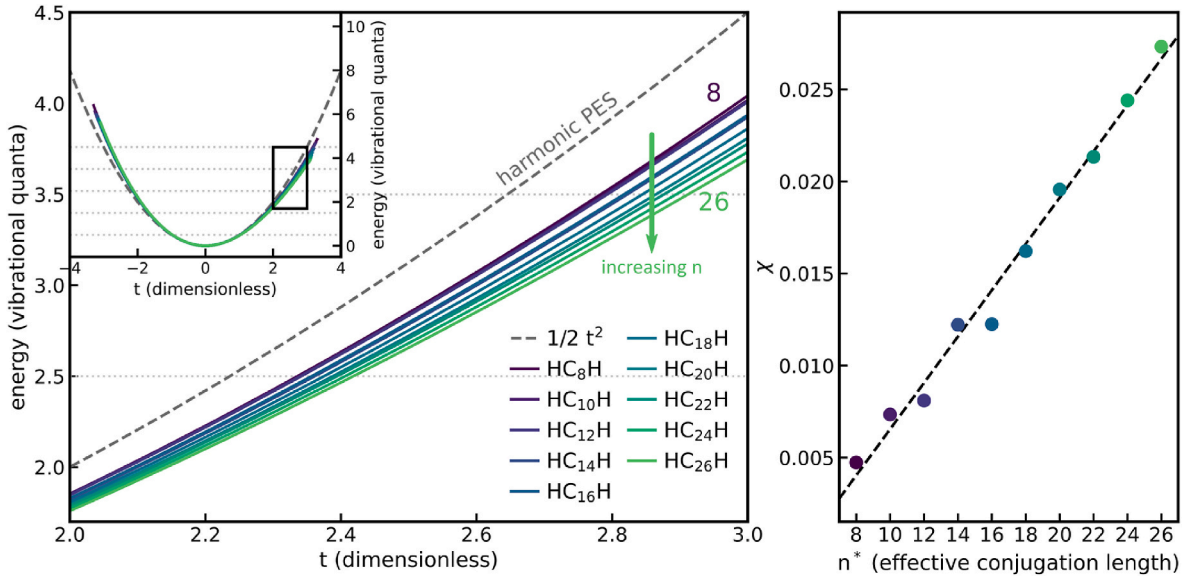

Fig. 8. a) Enlargement of the intra-molecular potential energy surface (PES) vs. the dimensionless ECC (α) coordinate *t* from DFT calculations on HC_nH polyynes in a range of *t* values explored during the classical trajectories corresponding to a few quanta-excited vibrational states. The entire PESs are reported in the inset, where the black rectangle indicates the zoomed region. The energy is measured in units of (harmonic) vibrational quanta. The dashed curve describes the ideal harmonic potential well. The phase of the *t* (q_α) coordinate is defined such that positive *t* values imply the stretching of the triple bonds and the shrinking of the single bonds. b) Nondimensional anharmonic parameter χ vs. n^* determined for HCnH from DFT calculations.

χ for the HC_nH series. As illustrated in the SI, a fit of $\overline{V}$ with the following polynomial expansion

$$\overline{V}(t) = \frac{1}{2}t^2 + \frac{1}{6}at^3 + \frac{1}{24}bt^4 \quad \text{(Eq. 4)}$$

allows a theoretical estimate of χ according to this expression

$$\chi = \frac{5}{6}a^2 - \frac{b}{4} \quad \text{(Eq. 5)}$$

In Table S5, we compare the values of χ determined for HC_nH through DFT calculations with the corresponding experimental values previously discussed. The experimental and theoretical results provide the same order of magnitude for χ and its increase with n^*. However, the calculations tend to overestimate the anharmonicity and predict a steeper rise with n^* (see Fig. 8b). These theoretical results, despite the well-known overestimation of the π electrons delocalization [2], contribute significantly to our understanding of the connection between anharmonicity and n^*. They confirm the general trends observed experimentally, further validating the robustness of the interpretation of experimental findings. Moreover, they highlight the importance of considering the connection between π-electron conjugation and anharmonicity of the ECC vibrational coordinate, which affects the transition from polyyne-like to cumulene-like structures.

4. Conclusions

We provide a thorough spectroscopic characterization of size-selected hydrogen-, methyl-, and cyano-capped carbon atomic wires (polyynes). We highlight the influence of size-confinements, *i.e.,* length and termination, on polyynes' π-electron conjugation. Moreover, our investigation gives valuable insight into the anharmonicity of the potential associated with the ECC mode. Thanks to the resonance conditions and the tunability of synchrotron radiation in the deep UV range, we were able to collect the resonance Raman spectra of diluted samples (down to $\approx 10^{-8}$ M), which would be otherwise undetectable using off-resonance Raman spectroscopy. Our work confirms the presence of methyl-capped polyynes, reporting for the first time their size-selected Raman spectra and validating their recognition as previously discussed in other experiments [36,55].

By integrating the analysis of UV–Vis absorption and UVRR spectra, we highlight that the cyano group significantly affects the π electrons of the carbon wire, extending the conjugation length and leading to a larger electron-phonon coupling compared to fully hydrogenated wires. The observation of two-quanta vibrational transitions allows us to shed light on the intriguing anharmonicity in short linear carbon chains for which confinement effects play a fundamental role. We theoretically estimate the nondimensional anharmonicity parameters χ, which agrees with the trend obtained through the experiments. Moreover, from UVRR experiments, we noticed an increase in the anharmonicity of hetero-terminated systems depending on the terminating group. This finding deserves further studies, focusing on the effect of the vibrational coupling with the capping group. For instance, analyzing dimethyl- ($CH_3-C_n-CH_3$) and dicyano-capped ($C\equiv N-C_n-C\equiv N$) systems would deepen the knowledge of the impact of terminations on anharmonicity.

From a fundamental point of view, the effective length marking the difference between short linear carbon chains, with size-confinement behavior, and carbyne-like systems, whose properties are independent of the size, would set the threshold between a bottom-up (i.e., molecular) and a top-down (i.e., solid state) approaches for one-dimensional carbon. We expect a saturation of the anharmonicity curve to reach a plateau representing the value for carbyne. In the case of the absorption features, this threshold has been estimated to be at about 68–72 carbon atoms [20]. The systems analyzed in this work are far from this limit, and we observe a linear dependence of the anharmonicity, showing that short wires can be exploited for the extreme tunability of these properties.

The potential of linear carbon atomic wires (polyynes and cumulenes) in advanced technology fields has been recently unveiled in a few proof-of-concept demonstrations [13,15,16,74,75]. The detailed understanding of the effect of length and termination and the ability to finely control polyynes' structure will allow us to fully exploit their unique conjugation effects and open new possibilities to properly engineer the properties of these systems for optical, electronic, and opto-electronic applications.

CRediT authorship contribution statement

P. Marabotti: Conceptualization, Methodology, Formal analysis, Investigation, Data curation, Writing – original draft, Visualization. **M. Tommasini:** Methodology, Software, Validation, Formal analysis, Resources, Data curation, Writing – review & editing, Visualization. **C. Castiglioni:** Methodology, Validation, Formal analysis, Resources, Writing – review & editing, Visualization. **S. Peggiani:** Conceptualization, Methodology, Validation, Investigation, Writing – review & editing. **P. Serafini:** Formal analysis. **B. Rossi:** Methodology, Investigation, Resources, Writing – review & editing. **A. Li Bassi:** Validation, Writing – review & editing, Supervision. **V. Russo:** Validation, Investigation, Writing – review & editing, Supervision. **C.S. Casari:** Conceptualization, Validation, Investigation, Resources, Data curation, Writing – review & editing, Supervision, Project administration, Funding acquisition.

Declaration of competing interest

The authors declare that they have no known competing financial interests or personal relationships that could have appeared to influence the work reported in this paper.

Acknowledgments

P.M., M.T., C.C., S.P., P.S., A.L.B., V.R., and C.S.C. acknowledge funding from the European Research Council (ERC) under the European Union's Horizon 2020 research and innovation program ERC Consolidator Grant (ERC CoG2016 EspLORE grant agreement no. 724610, www.esplore.polimi.it). We acknowledge Elettra Sincrotrone Trieste for providing access to its synchrotron radiation facilities and for financial support (proposal numbers 20205267 and 20215090).

Appendix A. Supplementary data

Supplementary data to this article can be found online at https://doi.org/10.1016/j.carbon.2023.118503.

References

[1] C.S. Casari, M. Tommasini, R.R. Tykwinski, A. Milani, Carbon-atom wires: 1-D systems with tunable properties, Nanoscale 8 (2016) 4414–4435, https://doi.org/10.1039/C5NR06175J.
[2] M. Tommasini, D. Fazzi, A. Milani, M. Del Zoppo, C. Castiglioni, G. Zerbi, Intramolecular vibrational force fields for linear carbon chains through an adaptative linear scaling scheme, J. Phys. Chem. A 111 (2007) 11645–11651, https://doi.org/10.1021/jp0757006.
[3] A. Milani, A. Lucotti, V. Russo, M. Tommasini, F. Cataldo, A. Li Bassi, et al., Charge transfer and vibrational structure of sp-hybridized carbon atomic wires probed by surface enhanced Raman spectroscopy, J. Phys. Chem. C 115 (2011) 12836–12843, https://doi.org/10.1021/jp203682c.
[4] A. Milani, V. Barbieri, A. Facibeni, V. Russo, A. Li Bassi, A. Lucotti, et al., Structure modulated charge transfer in carbon atomic wires, Sci. Rep. 9 (2019) 1648, https://doi.org/10.1038/s41598-018-38367-9.
[5] A. Milani, M. Tommasini, V. Barbieri, A. Lucotti, V. Russo, F. Cataldo, et al., Semiconductor-to-Metal transition in carbon-atom wires driven by sp ^{2} conjugated end groups, J. Phys. Chem. C 121 (2017) 10562–10570, https://doi.org/10.1021/acs.jpcc.7b02246.
[6] S. Tongay, R.T. Senger, S. Dag, S. Ciraci, A b - i n i t i o Electron Transport Calculations of Carbon Based String Structures, Phys. Rev. Lett. 93 (2004), 136404, https://doi.org/10.1103/PhysRevLett.93.136404.
[7] S. Yang, M. Kertesz, Bond length alternation and energy band gap of polyyne, J. Phys. Chem. A 110 (2006) 9771–9774, https://doi.org/10.1021/jp062701+.
[8] K. Zhang, Y. Zhang, L. Shi, A review of linear carbon chains, Chin. Chem. Lett. 31 (2020) 1746–1756, https://doi.org/10.1016/j.cclet.2020.03.019.
[9] W.A. Chalifoux, R.R. Tykwinski, Synthesis of polyynes to model the sp-carbon allotrope carbyne, Nat. Chem. 2 (2010) 967–971, https://doi.org/10.1038/nchem.828.
[10] E. Gao, R. Li, R.H. Baughman, Predicted confinement-enhanced stability and extraordinary mechanical properties for carbon nanotube wrapped chains of linear carbon, ACS Nano 14 (2020), 17071, https://doi.org/10.1021/acsnano.0c06602. –9.
[11] C.S. Casari, A. Milani, Carbyne: from the elusive allotrope to stable carbon atom wires, MRC 8 (2018) 207–219, https://doi.org/10.1557/mrc.2018.48.
[12] M.R. Bryce, A review of functional linear carbon chains (oligoynes, polyynes, cumulenes) and their applications as molecular wires in molecular electronics and optoelectronics, J. Mater. Chem. C 9 (2021) 10524–10546, https://doi.org/10.1039/D1TC01406D.
[13] S. Pecorario, A.D. Scaccabarozzi, D. Fazzi, E. Gutiérrez-Fernández, V. Vurro, L. Maserati, et al., Stable and solution-processable cumulenic sp-carbon wires: a new paradigm for organic electronics, Adv. Mater. 34 (2022), 2110468, https://doi.org/10.1002/adma.202110468.
[14] B. Standley, W. Bao, H. Zhang, J. Bruck, C.N. Lau, M. Bockrath, Graphene-based atomic-scale switches, Nano Lett. 8 (2008) 3345–3349, https://doi.org/10.1021/nl801774a.
[15] F. Hu, C. Zeng, R. Long, Y. Miao, L. Wei, Q. Xu, et al., Supermultiplexed optical imaging and barcoding with engineered polyynes, Nat. Methods 15 (2018) 194–200, https://doi.org/10.1038/nmeth.4578.
[16] A.D. Scaccabarozzi, A. Milani, S. Peggiani, S. Pecorario, B. Sun, R.R. Tykwinski, et al., A field-effect transistor based on cumulenic sp-carbon atomic wires, J. Phys. Chem. Lett. 11 (2020) 1970, https://doi.org/10.1021/acs.jpclett.0c00141. –4.
[17] M. Liu, V.I. Artyukhov, H. Lee, F. Xu, B.I. Yakobson, Carbyne from first principles: chain of C atoms, a nanorod or a nanorope, ACS Nano 7 (2013) 10075–10082, https://doi.org/10.1021/nn404177r.
[18] A.L. Torre, A. Botello-Mendez, W. Baaziz, J.-C. Charlier, F. Banhart1, Strain-induced metal–semiconductor transition observed in atomic carbon chains, Nat. Commun. 6 (2015) 6636, https://doi.org/10.1038/ncomms7636.
[19] D. Romanin, L. Monacelli, R. Bianco, I. Errea, F. Mauri, M. Calandra, Dominant role of quantum anharmonicity in the stability and optical properties of infinite linear acetylenic carbon chains, J. Phys. Chem. Lett. 12 (2021) 10339–10345, https://doi.org/10.1021/acs.jpclett.1c02964.
[20] Y. Gao, Y. Hou, F. Gordillo Gámez, M.J. Ferguson, J. Casado, R.R. Tykwinski, The loss of endgroup effects in long pyridyl-endcapped oligoynes on the way to carbyne, Nat. Chem. 12 (2020) 1143–1149, https://doi.org/10.1038/s41557-020-0550-0.
[21] A. Milani, M. Tommasini, V. Russo, A. Li Bassi, A. Lucotti, F. Cataldo, et al., Raman spectroscopy as a tool to investigate the structure and electronic properties of carbon-atom wires, Beilstein J. Nanotechnol. 6 (2015) 480–491, https://doi.org/10.3762/bjnano.6.49.
[22] P. Marabotti, A. Milani, A. Lucotti, L. Brambilla, M. Tommasini, C. Castiglioni, et al., Vibrational and nonlinear optical properties of amine-capped push-pull polyynes by infrared and Raman spectroscopy, Carbon Trends 5 (2021), 100115, https://doi.org/10.1016/j.cartre.2021.100115.
[23] N.R. Agarwal, A. Lucotti, D. Fazzi, M. Tommasini, C. Castiglioni, W.A. Chalifoux, et al., Structure and chain polarization of long polyynes investigated with infrared and Raman spectroscopy: investigation of long polyynes with infrared and Raman spectroscopy, J. Raman Spectrosc. 44 (2013) 1398–1410, https://doi.org/10.1002/jrs.4300.
[24] G. Compagnini, V. Mita, L. D'Urso, R.S. Cataliotti, O. Puglisi, Spectroscopic study of polyynes obtained by laser ablation in liquids, J. Raman Spectrosc. 39 (2008) 177–181, https://doi.org/10.1002/jrs.1837.
[25] H. Tabata, M. Fujii, S. Hayashi, T. Doi, T. Wakabayashi, Raman and surface-enhanced Raman scattering of a series of size-separated polyynes, Carbon 44 (2006) 3168–3176, https://doi.org/10.1016/j.carbon.2006.07.004.
[26] P. Marabotti, S. Peggiani, A. Facibeni, P. Serafini, A. Milani, V. Russo, et al., In situ surface-enhanced Raman spectroscopy to investigate polyyne formation during pulsed laser ablation in liquid, Carbon 189 (2022) 219–229, https://doi.org/10.1016/j.carbon.2021.12.060.
[27] U. Szczepaniak, K. Ozaki, K. Tanaka, Y. Ohnishi, Y. Wada, J.-C. Guillemin, et al., Phosphorescence excitation mapping and vibrational spectroscopy of HC9N and HC11N cyanopolyynes in organic solvents, J. Mol. Struct. 1214 (2020), 128201, https://doi.org/10.1016/j.molstruc.2020.128201.
[28] F. Innocenti, A. Milani, C. Castiglioni, Can Raman spectroscopy detect cumulenic structures of linear carbon chains? J. Raman Spectrosc. (2009) https://doi.org/10.1002/jrs.2413 n/a-n/a.
[29] S. Heeg, L. Shi, L.V. Poulikakos, T. Pichler, L. Novotny, Carbon nanotube chirality determines properties of encapsulated linear carbon chain, Nano Lett. 18 (2018) 5426–5431, https://doi.org/10.1021/acs.nanolett.8b01681.
[30] R.B. Heimann, S.E. Evsyukov, L. Kavan, Carbyne and Carbynoid Structures, Springer Netherlands, Dordrecht, 1999.
[31] S. Schrettl, E. Contal, T.N. Hoheisel, M. Fritzsche, S. Balog, R. Szilluweit, et al., Facile synthesis of oligoyne amphiphiles and their rotaxanes, Chem. Sci. 6 (2015) 564–574, https://doi.org/10.1039/C4SC03154G.
[32] A. Lucotti, M. Tommasini, D. Fazzi, M. Del Zoppo, W.A. Chalifoux, R.R. Tykwinski, et al., Absolute Raman intensity measurements and determination of the vibrational second hyperpolarizability of adamantyl endcapped polyynes: vibrational second hyperpolarizability of polyynes, J. Raman Spectrosc. 43 (2012) 1293–1298, https://doi.org/10.1002/jrs.3166.
[33] M. de Wergifosse, B. Champagne, Electron correlation effects on the first hyperpolarizability of push–pull π-conjugated systems, J. Chem. Phys. 134 (2011), 074113, https://doi.org/10.1063/1.3549814.
[34] F. Cataldo, O. Ursini, A. Milani, C.S. Casari, One-pot synthesis and characterization of polyynes end-capped by biphenyl groups (α,ω-biphenylpolyynes), Carbon 126 (2018) 232–240, https://doi.org/10.1016/j.carbon.2017.09.098.
[35] M. Tommasini, A. Milani, D. Fazzi, A. Lucotti, C. Castiglioni, J.A. Januszewski, et al., π-Conjugation and end group effects in long cumulenes: Raman spectroscopy and DFT calculations, J. Phys. Chem. C 118 (2014) 26415–26425, https://doi.org/10.1021/jp509724d.
[36] S. Peggiani, P. Marabotti, R.A. Lotti, A. Facibeni, P. Serafini, A. Milani, et al., Solvent-dependent termination, size and stability in polyynes synthesized *via* laser

ablation in liquids, Phys. Chem. Chem. Phys. 22 (2020) 26312–26321, https://doi.org/10.1039/D0CP04132G.
[37] S. Peggiani, A. Facibeni, A. Milani, C. Castiglioni, V. Russo, A. Li Bassi, et al., *In situ* synthesis of polyynes in a polymer matrix *via* pulsed laser ablation in a liquid, Mater Adv 1 (2020) 2729–2736, https://doi.org/10.1039/D0MA00545B.
[38] S. Peggiani, A. Senis, A. Facibeni, A. Milani, P. Serafini, G. Cerrato, et al., Size-selected polyynes synthesised by submerged arc discharge in water, Chem. Phys. Lett. 740 (2020), 137054, https://doi.org/10.1016/j.cplett.2019.137054.
[39] P. Marabotti, S. Peggiani, A. Vidale, C.S. Casari, Pulsed laser ablation in liquid of sp-carbon chains: status and recent advances, Chin. Phys. B 31 (2022), 125202, https://doi.org/10.1088/1674-1056/ac81b2.
[40] A. Lucotti, M. Tommasini, M.D. Zoppo, C. Castiglioni, G. Zerbi, F. Cataldo, et al., Raman and SERS investigation of isolated sp carbon chains, Chem. Phys. Lett. 417 (2006) 78–82, https://doi.org/10.1016/j.cplett.2005.10.016.
[41] G. Compagnini, G. Patanè, L. D'Urso, O. Puglisi, R.S. Cataliotti, B. Pignataro, On the interaction of carbon nanowires with noble metals through a study of their surface-enhanced Raman spectra, J. Phys. Chem. C 112 (2008) 20301–20306, https://doi.org/10.1021/jp807969c.
[42] L.M. Malard, D. Nishide, L.G. Dias, R.B. Capaz, A.P. Gomes, A. Jorio, et al., Resonance Raman study of polyynes encapsulated in single-wall carbon nanotubes, Phys. Rev. B 76 (2007), 233412, https://doi.org/10.1103/PhysRevB.76.233412.
[43] T. Wakabayashi, H. Tabata, T. Doi, H. Nagayama, K. Okuda, R. Umeda, et al., Resonance Raman spectra of polyyne molecules C10H2 and C12H2 in solution, Chem. Phys. Lett. 433 (2007) 296–300, https://doi.org/10.1016/j.cplett.2006.11.077.
[44] P. Marabotti, M. Tommasini, C. Castiglioni, P. Serafini, S. Peggiani, M. Tortora, et al., Electron-phonon coupling and vibrational properties of size-selected linear carbon chains by resonance Raman scattering, Nat. Commun. 13 (2022) 5052, https://doi.org/10.1038/s41467-022-32801-3.
[45] M. Martinati, W. Wenseleers, L. Shi, S.M. Pratik, P. Rohringer, W. Cui, et al., Electronic structure of confined carbyne from joint wavelength-dependent resonant Raman spectroscopy and density functional theory investigations, Carbon 189 (2022) 276–283, https://doi.org/10.1016/j.carbon.2021.12.059.
[46] N.F. Andrade, T.L. Vasconcelos, C.P. Gouvea, B.S. Archanjo, C.A. Achete, Y.A. Kim, et al., Linear carbon chains encapsulated in multiwall carbon nanotubes: resonance Raman spectroscopy and transmission electron microscopy studies, Carbon 90 (2015) 172–180, https://doi.org/10.1016/j.carbon.2015.04.001.
[47] T.A. Moura, W.Q. Neves, R.S. Alencar, Y.A. Kim, M. Endo, T.L. Vasconcelos, et al., Resonance Raman spectroscopy characterization of linear carbon chains encapsulated by multi-walled carbon nanotubes, Carbon 212 (2023), 118123, https://doi.org/10.1016/j.carbon.2023.118123.
[48] W. Chang, F. Liu, Y. Liu, T. Zhu, L. Fang, Q. Li, et al., Smallest carbon nanowires made easy: long linear carbon chains confined inside single-walled carbon nanotubes, Carbon 183 (2021) 571–577, https://doi.org/10.1016/j.carbon.2021.07.037.
[49] C.D. Tschannen, G. Gordeev, S. Reich, L. Shi, T. Pichler, M. Frimmer, et al., Raman scattering cross section of confined carbyne, Nano Lett. 20 (2020) 6750–6755, https://doi.org/10.1021/acs.nanolett.0c02632.
[50] L. Ravagnan, G. Bongiorno, D. Bandiera, E. Salis, P. Piseri, P. Milani, et al., Quantitative evaluation of sp/sp2 hybridization ratio in cluster-assembled carbon films by in situ near edge X-ray absorption fine structure spectroscopy, Carbon 44 (2006) 1518–1524, https://doi.org/10.1016/j.carbon.2005.12.015.
[51] B. Rossi, C. Bottari, S. Catalini, F. D'Amico, A. Gessini, C. Masciovecchio, Molecular and laser spectroscopy, in: Synchrotron-based Ultraviolet Resonance Raman Scattering for Material Science, Elsevier, 2020, pp. 447–482, https://doi.org/10.1016/B978-0-12-818870-5.00013-7.
[52] M.J. Frisch, G.W. Trucks, H.B. Schlegel, G.E. Scuseria, M.A. Robb, J.R. Cheeseman, et al., Gaussian 9 (2009).
[53] P. Serafini, Density Functional Theory Simulations as an Effective Tool to Investigate Optical, Electronic and Vibrational Properties of Sp and Hybrid Sp-Sp2 Carbon-Based Materials, PhD Thesis, Politecnico di Milano, 2022.
[54] F. Cataldo, Cyanopolyynes: carbon chains formation in a carbon arc mimicking the formation of carbon chains in the circumstellar medium, Int J Atrobiol 3 (2004) 237–246, https://doi.org/10.1017/S1473550404002149.
[55] A. Ramadhan, M. Wesolowski, T. Wakabayashi, H. Shiromaru, T. Fujino, T. Kodama, et al., Synthesis of hydrogen- and methyl-capped long-chain polyynes by intense ultrashort laser pulse irradiation of toluene, Carbon 118 (2017) 680–685, https://doi.org/10.1016/j.carbon.2017.03.096.
[56] T. Wakabayashi, M. Saikawa, Y. Wada, T. Minematsu, Isotope scrambling in the formation of cyanopolyynes by laser ablation of carbon particles in liquid acetonitrile, Carbon 50 (2012) 47–56, https://doi.org/10.1016/j.carbon.2011.07.053.
[57] L. Shi, P. Rohringer, K. Suenaga, Y. Niimi, J. Kotakoski, J.C. Meyer, et al., Confined linear carbon chains as a route to bulk carbyne, Nat. Mater. 15 (2016) 634–639, https://doi.org/10.1038/nmat4617.
[58] T. Vijayakumar, I.H. Joe, C.R. Nair, V. Jayakumar, Efficient π electrons delocalization in prospective push–pull non-linear optical chromophore 4-[N, N-dimethylamino]-4'-nitro stilbene (DANS): a vibrational spectroscopic study, Chem. Phys. 343 (2008) 83–99, https://doi.org/10.1016/j.chemphys.2007.10.033.
[59] J.P. Abraham, D. Sajan, V. Shettigar, S.M. Dharmaprakash, I. Němec, I. Hubert Joe, et al., Efficient π-electron conjugated push–pull nonlinear optical chromophore 1-(4-methoxyphenyl)-3-(3,4-dimethoxyphenyl)-2-propen-1-one: a vibrational spectral study, J. Mol. Struct. 917 (2009) 27–36, https://doi.org/10.1016/j.molstruc.2008.06.031.
[60] R.D. Johnson III, NIST Computational Chemistry Comparison and Benchmark Database, NIST Standard Reference Database Number, vol. 101, 2022.
[61] K. Wang, J. Liu, J. Yin, E. Aydin, G.T. Harrison, W. Liu, et al., Defect passivation in perovskite solar cells by cyano-based π-conjugated molecules for improved performance and stability, Adv. Funct. Mater. 30 (2020), 2002861, https://doi.org/10.1002/adfm.202002861.
[62] F. Bureš, O. Pytela, M. Kivala, F. Diederich, Solvatochromism as an efficient tool to study N,N-dimethylamino- and cyano-substituted π-conjugated molecules with an intramolecular charge-transfer absorption, J. Phys. Org. Chem. 24 (2011) 274–281, https://doi.org/10.1002/poc.1744.
[63] H. Li, M. Fang, Y. Hou, R. Tang, Y. Yang, C. Zhong, et al., Different effect of the additional electron-withdrawing cyano group in different conjugation bridge: the adjusted molecular energy levels and largely improved photovoltaic performance, ACS Appl. Mater. Interfaces 8 (2016) 12134–12140, https://doi.org/10.1021/acsami.6b00226.
[64] M.S. Liu, X. Jiang, S. Liu, P. Herguth, A.K.-Y. Jen, Effect of cyano substituents on electron affinity and electron-transporting properties of conjugated polymers, Macromolecules 35 (2002) 3532–3538, https://doi.org/10.1021/ma011790f.
[65] K. Tsukamoto, K. Takagi, S. Nagano, M. Hara, Y. Ie, K. Osakada, et al., π-Extension of electron-accepting dithiarubicene with a cyano-substituted electron-withdrawing group and application in air-stable n-channel organic field effect transistors, J. Mater. Chem. C 7 (2019) 12610–12618, https://doi.org/10.1039/C9TC04325J.
[66] A.M. Kelley, Resonance Raman overtone intensities and electron–phonon coupling strengths in semiconductor nanocrystals, J. Phys. Chem. A 117 (2013) 6143–6149, https://doi.org/10.1021/jp400240y.
[67] F. Negri, E. di Donato, M. Tommasini, C. Castiglioni, G. Zerbi, K. Müllen, Resonance Raman contribution to the *D* band of carbon materials: modeling defects with quantum chemistry, J. Chem. Phys. 120 (2004) 11889–11900, https://doi.org/10.1063/1.1710853.
[68] C. Ting, Polarized Raman spectra—I. Selection rules, Spectrochim. Acta Mol. Spectros 24 (1968) 1177–1189, https://doi.org/10.1016/0584-8539(68)80138-2.
[69] F.A.C. Oliveira, L.A. Cury, A. Righi, R.L. Moreira, P.S.S. Guimarães, F.M. Matinaga, et al., Temperature effects on the vibronic spectra of BEH–PPV conjugated polymer films, J. Chem. Phys. 119 (2003) 9777–9782, https://doi.org/10.1063/1.1615959.
[70] G. Grosso, G. Pastori Parravicini, Solid State Physics, second ed., Academic Press, an imprint of Elsevier, Amsterdam, 2014.
[71] A.C. Albrecht, On the theory of Raman intensities, J. Chem. Phys. 34 (1961) 1476–1484, https://doi.org/10.1063/1.1701032.
[72] P.M. Morse, Diatomic molecules according to the wave mechanics. II. Vibrational levels, Phys. Rev. 34 (1929) 57, https://doi.org/10.1103/PhysRev.34.57.
[73] M. Mendolicchio, J. Bloino, V. Barone, Perturb-then-diagonalize vibrational engine exploiting curvilinear internal coordinates, J. Chem. Theor. Comput. 18 (2022) 7603–7619, https://doi.org/10.1021/acs.jctc.2c00773.
[74] C.D. Tschannen, M. Frimmer, G. Gordeev, T.L. Vasconcelos, L. Shi, T. Pichler, et al., Anti-Stokes Raman scattering of single carbyne chains, ACS Nano 15 (2021) 12249–12255, https://doi.org/10.1021/acsnano.1c03893.
[75] Casari CS, Facibeni A, Peggiani S, Vidale A, Bertarelli C, Milani A. Etichetta anticontraffazione per l'autenticazione di beni, n.d..